Research Article

Journal of
Environmental
Nanotechnology

Sustainable Synthesis, Characterization and Adsorptive Application of Rice Husk-derived Magnesium Oxide Nanocomposites for Congo Red Removal from Aqueous Solutions

N. Krishnamoorthy[1], P. Rasagopal[2], V. M. Madhavan[3], J. Jenshya[4], S. Balachandran[5] and R. Girimurugan[6*]

[1]Department of Computer Applications (MCA), SRM Institute of Science and Technology, Chennai, TN, India
[2]Department of Mechanical Engineering, K.S.R. College of Engineering, Tiruchengode, TN, India
[3]Department of Mechanical Engineering, Sona College of Technology, Salem, TN, India
[4]Department of Computer Science and Engineering, Nandha College of Technology, Perundurai, TN, India
[5]Department of Chemical Engineering, Vel Tech High Tech Dr. Rangarajan Dr. Sakunthala Engineering College, Chennai, TN, India
[6]Department of Mechanical Engineering, Nandha College of Technology, Perundurai, TN, India
Received: 07.07.2026 Accepted: 09.08.2026 Published: 30.09.2026
*girinctmech@gmail.com

ABSTRACT

Water pollution continues to be a major global issue in the twenty-first century, requiring sophisticated and sustainable technology to safeguard human health, improve water quality, and conserve aquatic ecosystems. This work examines eco-friendly manufacture of magnesium oxide nanoparticles using rice husk as sustainable biomass source and assesses their efficacy in adsorbing Congo Red from aqueous solutions. Four MgO–rice husk nanocomposites, labeled RH–MgO-1, RH–MgO-2, RHB–MgO-1, and RHB–MgO-2, were synthesized and characterized through Fourier transform infrared spectroscopy, X-ray diffraction and scanning electron microscopy, to analyze their morphological, structural, and crystalline properties. Batch adsorption tests indicated optimal pH values of 8.5 for RH–MgO-1 (37.8 mg/g), 9.0 for RH–MgO-2 (39.0 mg/g), and 9.5 for both RHB–MgO-1 (43.6 mg/g) and RHB–MgO-2 (45.1 mg/g). The adsorption capabilities were determined using an adsorbent dosage of 0.05 g and contact duration of 45 minutes. The maximum adsorption capacities of 44.7, 58.2, 73.8, and 79.2 mg/g were attained for RH–MgO-1, RH–MgO-2, RHB–MgO-1, and RHB–MgO-2, respectively. Pseudo-first-order model yielded optimal fit for experimental data, whereas Langmuir model effectively characterized adsorption equilibrium, suggesting primarily monolayer adsorption. Thermodynamic evaluation verified that the process was spontaneous and exothermic. The impact of prevalent textile wastewater electrolytes ($AlCl_3 \cdot 6H_2O$ and NaCl, $CaCl_2 \cdot 2H_2O$) at concentrations from 0.05 to 0.50 M, alongside heavy metal ions (lead and chromium) at 40 to 200 ppm, on the adsorption efficacy of Congo Red dye was systematically examined. Findings indicate that the synthesized MgO–rice husk nanocomposites are economical, eco-friendly, and highly effective adsorbents, possessing considerable potential for sustainable remediation of dye-contaminated wastewater.

Keywords: MgO nanoparticles; Rice husk; Congo Red removal; Thermodynamics; Sustainable biomass.

1. INTRODUCTION

The continuous discharge of synthetic dyes from textile, leather, paper, and printing industries poses a serious environmental challenge because of toxicity, persistence, and resistance to biodegradation. Congo Red (CR) is a hazardous anionic azo dye with high stability, carcinogenicity, and adverse ecological impacts. Conventional treatment methods often suffer from high costs, incomplete removal, or secondary pollution, making adsorption one of the most effective and economical approaches for dye-contaminated wastewater treatment. Among various adsorbents, MgO nanoparticles have gained considerable attention owing to high surface basicity, chemical stability, non-toxicity, and abundant active adsorption sites. However, particle agglomeration and limited surface area restrict the performance of pure MgO. Consequently, MgO has been integrated with porous supports, carbonaceous materials, and metal oxide composites to enhance its surface properties, adsorption efficiency, and structural stability.

Several MgO-based nanocomposites have demonstrated remarkable adsorption and photocatalytic performances. Rice husk-derived silica was successfully employed to fabricate MFI zeolite-supported MgO nanoparticles, where the porous zeolite framework enhanced charge separation and enabled nearly 80% Methylene Blue (MB) photodegradation under UV irradiation(Albouyeh *et al.* 2020). Likewise, a green

hydrothermal Ag_2O/MgO/rice husk ash composite synthesized using plant extracts exhibited excellent crystallinity, stable dielectric behavior, and broad-spectrum antibacterial activity without compromising structural integrity (Sasikumar *et al.* 2026). An MgO/graphene oxide nanocomposite prepared by the solvothermal route achieved 97.84% Congo Red removal with an adsorption capacity of 684.85 mg g^{-1}, following Freundlich isotherm and pseudo-second-order kinetic model (Guo and Bulin, 2021). Similarly, mesoporous MgO/g-C_3N_4 composites were synthesized and characterized by XRD, BET, FESEM, HRTEM, XPS, and FTIR, confirming high surface area and favorable morphology. The composite exhibited maximum adsorption capacities of 1250 mg g^{-1} for Congo Red and 1791 mg g^{-1} for Basic Fuchsin, following the Langmuir isotherm and pseudo-second-order kinetics (Modwi *et al.* 2022).

In another study, a ZnO/MgO nanocomposite synthesized using Pechini sol–gel method displayed a maximum CR adsorption capacity of 317.46 mg g^{-1}, excellent reusability, and adsorption behavior consistent with the Langmuir isotherm and pseudo-second-order kinetics. The nanocomposite exhibited BET surface area of 58.72 m^2 g^{-1}, crystallite size of 87.56 nm, and SEM particle size of ~372.77 nm. The material achieved a maximum CR adsorption capacity of 317.46 mg g^{-1} at pH 2 within 90 minutes, following the Langmuir and pseudo-second-order models with excellent reusability (Alghanmi and Abdelrahman, 2024). Palm leaf biochar-functionalized MgO nanoparticles were characterized using FTIR, SEM, BET, and TGA, revealing a surface area increase from 2 to 178 m^2 g^{-1} with enhanced mesoporosity. The adsorbent achieved ~99% CR removal at pH 4 using 0.03 g adsorbent, exhibited a Langmuir capacity of 23.4 mg g^{-1}, and retained >89% efficiency after four regeneration cycles (Alfajri *et al.* 2026).

Green synthesis has emerged as an environmentally sustainable strategy for developing multifunctional MgO-based nanomaterials. Biogenic Ag-doped MgO nanocomposites synthesized using *Eucalyptus globulus* leaf extract exhibited a reduced optical bandgap together with 97.9% Congo Red degradation, complete Malachite Green degradation, and significantly enhanced antibacterial activity (Begum *et al.* 2025). Similarly, algal biochar-supported Ag nanocomposite was characterized by BET, FESEM-EDX, FTIR, XRD, XPS, and TGA, confirming a mesoporous, thermostable structure with abundant active functional groups. The adsorbent achieved 95.92% CR removal (q_e = 34.53 mg g^{-1}) at pH 6 within 60 minutes, and maintained effective performance over five adsorption–desorption cycles (Shaikh *et al.* 2022a). These findings show synergistic benefits obtained through green synthesis and biomass-assisted nanocomposite fabrication.

Besides nanocomposites, low-cost agricultural residues have also been utilized to produce sustainable adsorbents for dye removal. For example, activated carbon derived from *Sterculia foetida* shells demonstrated effective removal of Acid Blue 158 dye (Rajesh *et al.* 2024). Rice straw fibres were characterized using FTIR, HR-XRD, FESEM-EDS, BET, and pH_pzc, demonstrating their suitability as lignocellulosic biosorbents. Maximum removal efficiencies of 88.7% (Malachite Green), 87.5% (MB), 82.87% (Basic Fuchsin), and 22.2% (CR) were obtained with cationic dye adsorption following Langmuir isotherm and second-order (Gupta and Dey, 2025). Powdered *Spathodea campanulata* leaves were employed as a low-cost biosorbent for CR removal, and process variables were optimized using response surface methodology. The optimized conditions yielded a maximum CR removal efficiency of 88.2%, demonstrating the effectiveness of this sustainable biosorbent (Ravikumar and King, 2020). A magnetic biosorbent derived from *Phragmites australis* was characterized using SEM and FTIR to evaluate its morphology and surface functional groups. Material achieved 97% CR removal with maximum adsorption of 3.36 mg g^{-1}, reached an equilibrium within 180 minutes, and followed Langmuir isotherm and second-order kinetic model (Abdallah and Alprol, 2024).

Recent studies have further emphasized importance of sustainable nanomaterials with enhanced adsorption performance. Green-synthesized Mn nanoparticles derived from pine needle extract were characterized for morphology, surface functional groups, and textural properties prior to Methylene Blue adsorption. Adsorption followed pseudo-second-order model (R^2 = 0.9983) and Freundlich isotherm (R^2 = 0.9931), with $\Delta H° = -32.02$ kJ mol^{-1} and $\Delta G° < 0$, confirming a spontaneous and exothermic physisorption process (Ameen *et al.* 2026). Graphene-like porous carbon synthesized from walnut shell waste showed BET surface area of 45 m^2 g^{-1}, pore volume of 6.94 cm^3 g^{-1}, and average pore diameter of 4.73 nm, confirming a mesoporous structure. The adsorbent achieved maximum adsorption capacities of 83.53 mg g^{-1} (diclofenac), 40.68 mg g^{-1} (ciprofloxacin), and 40.57 mg g^{-1} (tetracycline), following Langmuir isotherm and pseudo-second-order kinetics, while MLP model predicted adsorption with R^2 = 0.98–1.00 (Sabherwal *et al.* 2026). Similarly, green ZnO nanoparticles synthesized by *Mangifera indica* and *Syzygium cumini* leaf extracts achieved 99% Methyl Red removal with excellent regeneration capability (Inam *et al.* 2025). Furthermore, polypyrrole-coated TiB_2 nanoparticles exhibited 98.75% Congo Red removal together with excellent adsorption stability during repeated adsorption–desorption cycles (Mayakannan *et al.* 2022).

Although numerous MgO-based composites and biomass-derived adsorbents have been reported, relatively few studies have systematically investigated

green-synthesized MgO nanocomposites derived from rice husk processed through different biomass modification routes, including raw biomass, alkali-treated biomass, and biochar produced at different pyrolysis temperatures. Moreover, comprehensive evaluations integrating adsorption optimization, kinetic modeling, equilibrium isotherms, thermodynamic analysis, electrolyte effects, heavy metal interference, desorption behavior, and reusability remain limited. Therefore, the present study develops eco-friendly MgO–rice husk nanocomposites using raw rice husk, alkali-treated rice husk, and rice husk biochars prepared at different pyrolysis temperatures as sustainable biomass supports. The synthesized nanocomposites are comprehensively characterized using XRD, FTIR, and SEM followed by systematic evaluation of CR adsorption under varying operating conditions. Adsorption behavior is further interpreted using kinetic, equilibrium, and thermodynamic models together with regeneration and interference studies to establish the potential of these sustainable MgO–rice husk nanocomposites for practical wastewater remediation.

2. MATERIALS AND METHODS

2.1 Materials

Congo Red dye, magnesium nitrate hexahydrate [$Mg(NO_3)_2 \cdot 6H_2O$] and ethanol were obtained from Star Scientific, Erode, Tamil Nadu, India. Rice husk was sourced from local rice mills in Coimbatore, and utilized to fabricate four distinct MgO-based adsorbents: RH–MgO-1 (raw rice husk + MgO), RH–MgO-2 (alkali-treated rice husk + MgO), RHB–MgO-1 (rice husk biochar + MgO, pyrolyzed at 500 °C), and RHB–MgO-2 (rice husk biochar + MgO, pyrolyzed at 700 °C).

2.2 Raw Rice Husk Preparation

The harvested rice husk was meticulously rinsed with running water and subsequently with double-deionized water to eliminate dust and surface contaminants. Purified rice husk was air-dried for 5 days to eliminate residual moisture. Desiccated substance was pulverized into fine powder. About 1 g of this powder was subjected to treatment with 100 mL of 95% ethanol for roughly 3 hours under continuous agitation (Ali and Dreaa, 2023). The treated sample was thoroughly rinsed using double-deionized water and permitted to dry at fume hood for 2 hours. Material was subsequently oven-dried at 70 °C for 20 hours, yielding purified raw rice husk powder (RH), which was utilized for the synthesis of the RH–MgO-1 nanocomposite.

2.3 Alkali-treated Rice Husk Preparation

The purified and desiccated rice husk was submerged in 5 wt.% NaOH solution at room temperature for 4 hours to eliminate hemicellulose, lignin, waxes, and other contaminants from the biomass surface (Gaddala *et al.* 2025). The alkali-treated rice husk was subsequently rinsed multiple times with double-deionized water until neutral pH was achieved. Material was dried in hot-air oven at 70 °C for 20 hours, pulverized into fine powder, and stored in airtight container for the synthesis of the RH–MgO-2 nanocomposite.

2.4 Biochar Production from Rice Husk

The purified and desiccated rice husk was positioned in ceramic crucibles and subjected to pyrolysis in a muffle furnace under restricted oxygen conditions (Khasim *et al.* 2024). Two distinct pyrolysis temperatures were utilized to produce rice husk biochar samples. The initial batch was subjected to temperature of 500 °C at heating rate and held for 2 hours, resulting in RHB–MgO-1. Second batch underwent pyrolysis under the same circumstances at 700 °C for 2 hours to yield RHB–MgO-2. Upon natural cooling to ambient temperature, both biochar samples were pulverized into fine powders, passed through a 100-mesh filter, and preserved in airtight containers for the subsequent production of MgO nanoparticles.

2.5 Synthesis of MgO

Extracts of alkali-treated rice husk, raw rice husk, rice husk biochar pyrolyzed at 500 °C (RHB-500), and rice husk biochar at 700 °C (RHB-700) were produced by dispersing 10 g of each dried powder in 100 mL of distilled water. Suspensions were incubated at 40 °C for 24 hours with shaking at 50–70 rpm utilizing shaker. Subsequent to incubation, each extract was subjected to filtration by Whatman No. 1 filter paper to get clear filtrate.

In the green production of MgO nanocomposites, 20 mL of rice husk extract was individually combined with a 0.1 M magnesium nitrate hexahydrate solution while maintaining continuous magnetic stirring for 5 hours. The reaction mixtures were permitted to stand at ambient temperature for 24 hours, leading to the development of a white magnesium hydroxide precursor. The precipitates were obtained using centrifugation, thoroughly washed with distilled water and ethanol to eliminate contaminants, and dried at hot-air oven at 70 °C for 12 hours (Li *et al.* 2020). Dried powders were ultimately calcined in a muffle furnace at 450 °C for 3 hours to produce MgO nanocomposites, labeled as RH–MgO-1, RH–MgO-2, RHB–MgO-1, and RHB–MgO-2. The comprehensive synthesis protocol is shown in Fig. 1.

2.6 Congo Red Solution Preparation

Congo Red dye was used as the pollutant for the adsorption studies. A stock solution was prepared by dissolving 1 g of CR dye in 1 L of deionized water.

Working solutions with concentration between 20 and 180 mg/L were generated through precise dilution of stock solution (Raman *et al.* 2025). Absorbance of dye solutions was quantified by UV–Visible spectrophotometer (Shimadzu, Japan), and calibration curve was constructed at peak absorption wavelength (λ_{max} = 497 nm) for quantitative assessment. Fig. 2 illustrates the comprehensive preparation of the dye solutions.

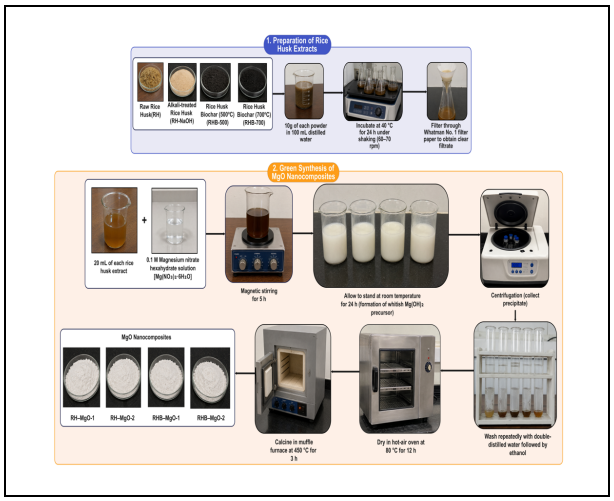

Fig. 1: Preparation of rice husk extract

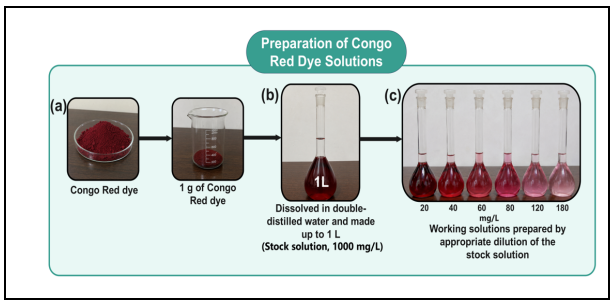

Fig. 2: (a) Congo red dye, (b) Stock dye solution and (c) Aqueous dye solutions

2.7 Adsorption Experimental Procedure

Adsorption efficacy of the synthesized MgO–rice husk nanocomposite adsorbents was assessed utilizing Congo Red dye as the model contaminant. Process parameters, like adsorbent dosage, initial dye concentration, pH, temperature, and contact duration were examined (Güllüce *et al.* 2026). The adsorption tests were conducted in 250 mL conical flasks, whereby 50 mL of CR dye was combined with requisite quantity of adsorbent. A pH of solution was modified utilizing 0.1 M NaOH and 0.1 M HCl solutions. Flasks was enveloped in aluminum foil and positioned in orbital shaker. The contact duration, pH, temperature, initial dye concentration and adsorbent dosage were changed within ranges of 2–11, 0.11–0.11 g, 6–60 minutes, 25–125 mg/L, and 35–65 °C. Following necessary contact duration, adsorbents were isolated *via* centrifugation at 5000 rpm, and the remaining dye concentration was quantified by UV–Visible spectrophotometer at λ_{max} = 497 nm (Abou *et al.* 2020). The equilibrium adsorption capacity was calculated using equation 1, which is the amount of adsorbate taken up by the adsorbent per unit mass at equilibrium.

$$qe = \frac{(C_o - C_e)V}{W} \quad \text{... (1)}$$

3. RESULTS AND DISCUSSION

3.1 Optimization Variables

3.1.1 Effect of Solution pH

The pH of solution is essential in regulating surface of ionization state of the adsorbate, therefore affecting adsorption process. Optimal pH values for the highest adsorption capabilities of RH–MgO-1, RH–MgO-2, RHB–MgO-1, and RHB–MgO-2 were identified as 8.5 (37.8 mg/g), 9.0 (39.0mg/g), 9.5 (43.6 mg/g), and 9.5 (45.1 mg/g), respectively. The adsorption efficacy of synthesized MgO–rice husk nanocomposites for CR dye was examined across a pH spectrum of 3.0 to 10.5. Likewise, in a previous study, *Tecoma stans* flower-derived MgO exhibited the highest adsorption capacity (150.49 mg g^{-1}) with 99.7% CR removal under optimum conditions (Nguyen *et al.* 2021). The pH was modified utilizing 0.1 M NaOH or 0.1 M HCl. The outcomes showed that alkaline circumstances enhanced adsorption of CR dye, with peak adsorption capabilities occurring at pH 8.5–9.5, as depicted in Fig. 3.

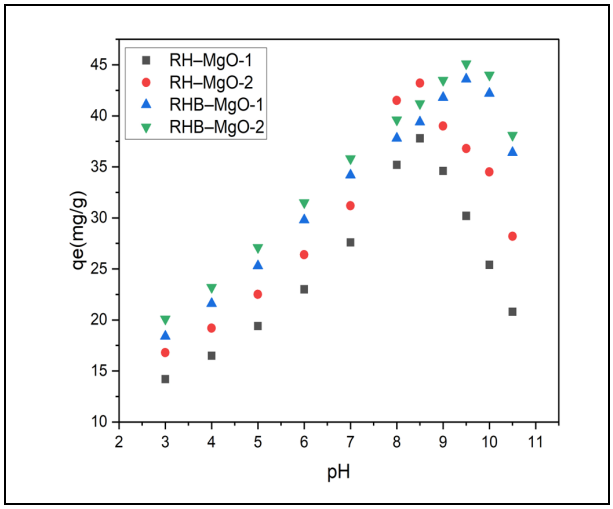

Fig. 3: Effect of solution pH on adsorption

Adsorption of Red XGRL utilizing polymeric nanocomposites indicated that optimal adsorption efficiency was attained within pH range 8–11. The data was ascribed to advantageous electrostatic interactions and the presence of active adsorption sites on adsorbent surface.

The current work reveals that the synthesized MgO–rice husk nanocomposites (RH–MgO-1, RH–MgO-2, RHB–MgO-1 and RHB–MgO-2) show significant adsorption capacities for Congo Red dye, achieving optimal adsorption capacities of 37.8, 39.0, 43.6, and 45.1 mg/g, respectively. The improved adsorption efficacy is due to synergistic effects of hydrogen bonding, surface complexation, and porous architecture of the MgO–rice husk composites, which offer numerous active sites for dye adsorption. The analysis of four distinct MgO-based adsorbents reveals their superior adsorption effectiveness, highlighting their potential as sustainable and eco-friendly materials for remediation of dye-contaminated wastewater.

3.1.2 Effect of biosorbent dose

The adsorption capability of the synthesized MgO–rice husk nanocomposites under varying operating conditions was crucial factor influencing the adsorption process. Influence of adsorbent dose on elimination of CR dye was examined within range 0.04–0.21 g per 50 mL of dye solution. Fig. 4 illustrates that adsorption capacity of synthesized nanocomposites fluctuated with augmentation of adsorbent dosage. The adsorption capabilities of the nanocomposites diminished progressively with the augmentation of adsorbent dose, attributed to overlap of active adsorption sites and aggregation of adsorbent particles. Under optimal operating conditions (pH 8–10, 35 °C, and 120 rpm), the adsorption capacities diminished from 47.1 to 27.0 mg/g for RH–MgO-1 and from 40.2 to 29.3 mg/g for RH–MgO-2, while analogous decreasing trends were noted for RHB–MgO-1 and RHB–MgO-2 as adsorbent dosage escalated from 0.04 to 0.21 g. Similarly, when Green CuO synthesized from *Polygonum sivasicum* extract was characterized under optimum conditions (pH 5, 328 K, 24 h,), the adsorbent achieved 89% tetracycline removal with Langmuir adsorption capacity of 217.39 mg g^{-1}, following pseudo-second-order kinetic model (Şentürk and Topal, 2026).

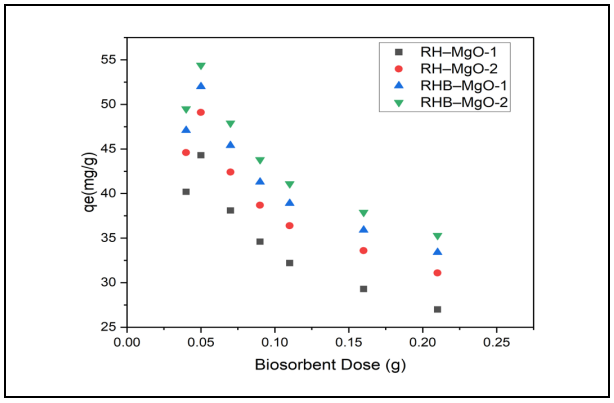

Fig. 4: Effect of biosorbent dose on adsorption

The optimal adsorbent dosage was established as 0.05 g per 50 mL of dye solution. A prior investigation (Khader *et al.* 2021) examined addition of adsorbent dosage on elimination of Drimaren Black CL-B dye by rice husk as biosorbent within the dose range of 0.05–0.30 g. The findings indicated that optimal adsorption occurred at 0.05 g; however, raise in adsorbent dose led to reduction in adsorption capacity because of particle aggregation and the overlap of active adsorption sites.

3.1.3 Effect on Contact Time

The primary factor in dye adsorption was duration of contact time between dye molecules and powder. The effects of contact time was examined within range of 10 to 65 minutes, and the results are presented in Fig. 5.

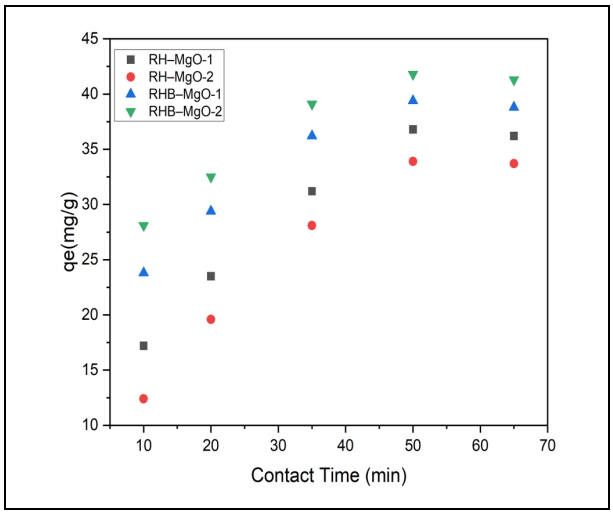

Fig. 5: Effect of contact time on adsorption

3.1.4 Effect on Temperature

The findings indicated that contact time significantly affected the adsorption efficacy of the synthesized MgO–rice husk nanocomposites for Congo Red dye. The adsorption process was rapid in first 20 minutes, then exhibited a progressive decline at adsorption rate as the active sites became occupied, until achieving equilibrium after 60 minutes. After 45 minutes, the adsorption capacities of RH–MgO-1, RH–MgO-2, RHB–MgO-1, and RHB–MgO-2 were 36.5, 39.0, 42.6, and 44.8 mg/g, respectively (Fig. 6). Consequently, 60 minutes were deemed optimal contact duration, as no substantial enhancement in adsorption capacity was noted beyond this timeframe.

The investigation indicated that the adsorption capacity surged swiftly during the initial phase and gradually attained equilibrium after 60 minutes, signifying the saturation of available adsorption sites.

The MgO–rice husk nanocomposites attained adsorption equilibrium in 60 minutes, exhibiting a significantly more rapid adsorption rate compared to a previously documented sawdust-based composite (Guo

and Bulin, 2021). RHB–MgO-2 achieved adsorption capacity of 40.3 mg/g in 60 minutes, demonstrating rapid absorption of CR molecules. Comprehensive analysis of the 5–60 minutes interval distinctly identified two separate adsorption stages: an initial rapid adsorption phase (0–20 minutes) characterized by numerous active surface sites, succeeded by a slower adsorption phase (20–60 minutes) linked to the gradual saturation of these sites and intraparticle diffusion. The relatively brief equilibrium period and elevated adsorption capacity indicate the potential of the synthesized MgO–rice husk nanocomposites as effective and sustainable adsorbents for the remediation of dye-contaminated wastewater.

Temperature affects adsorption capacity of adsorbent. Temperature on removal of basic CR dye was examined, maintaining all other variables constant within the range 35 to 65 °C. The results indicated exothermic nature of adsorption of basic CR dye, as dye removal capacity of biocomposites diminished from 37.2 to 32.2 mg/g and from 39.6 to 35.6 mg/g.

Diminished adsorption capacity at temperatures is due to attenuation of contacts between CR molecules and active adsorption sites, alongside the heightened kinetic dye molecules, which facilitates their desorption from the adsorbent surface. The results demonstrate that 35 °C was the optimal working temperature for maximizing adsorption of CR dye with synthesized MgO–rice husk nanocomposites.

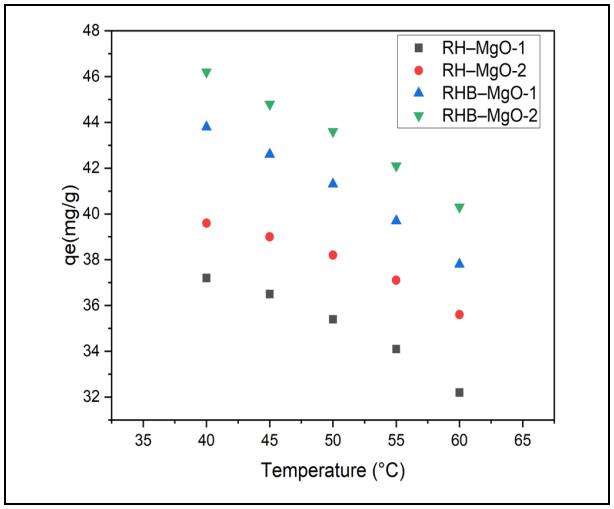

Fig. 6: Effect of temperature on adsorption

Adsorption of CR dye utilizing a MgO–graphene oxide (MgO–GO) composite within the 25–60 °C temperature range. The findings indicated that adsorption capacity diminished with rising temperature, signifying that adsorption process was exothermic. The adsorption capacity of RH–MgO-1 diminished from 37.2 to 32.2 mg/g at 35 °C to 65 °C, hence affirming the exothermic characteristic of the adsorption process. The synthesized MgO–rice husk nanocomposites, derived from inexpensive agricultural waste, offer a sustainable and eco-friendly alternative to synthetic MgO–GO composites, while exhibiting superior adsorption performance and distinct thermodynamic behavior appropriate for adsorption and thermodynamic analyses.

3.1.5 Effect on Dye Concentration

Dye concentration is a crucial factor affecting adsorption capacity of an adsorbent, as it dictates mass transfer force among dye molecules and adsorbent surface. Impact of initial Congo Red dye concentration was examined within the range of 35–130 mg/L under optimal adsorption conditions. The outcomes show that adsorption capability of the synthesized MgO–rice husk nanocomposites augmented with higher initial dye concentrations, attributable to the increased concentration gradient and elevated collision frequency between accessible adsorption sites and dye molecules. Highest adsorption capacities were 44.7 mg/g for RH–MgO-1 at dye concentration of 100 mg/L, whereas RH–MgO-2, RHB–MgO-1, and RHB–MgO-2 had maximum adsorption capacity of 58.2, 73.8, and 79.2 mg/g, respectively, at dye concentration of 130 mg/L. All adsorption experiments was performed at the previously adjusted conditions, and outcomes are illustrated in Fig. 7. The current research quantitatively assessed the adsorption capabilities of four distinct MgO–rice husk nanocomposites.

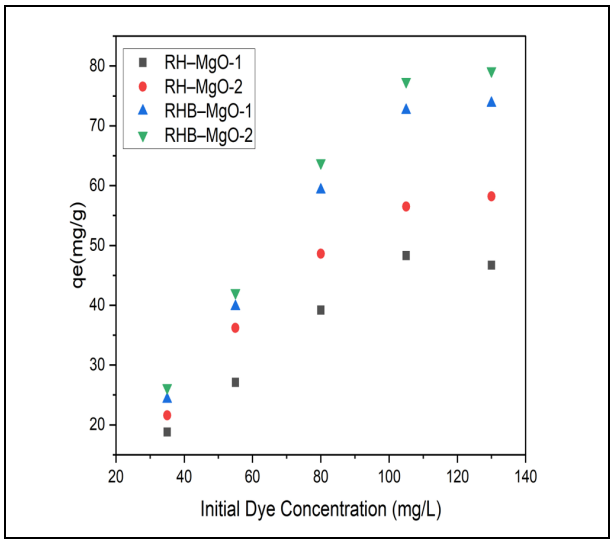

Fig. 7: Effect of initial dye concentration

Adsorption tests utilized dye concentrations between 20 and 100 ppm, with an adsorbent dosage of 0.01 g. Their findings showed that adsorption capacity raised with higher initial dye concentration because of augmented mass transfer driving force between adsorbent surface and dye molecules. Among synthesized adsorbents, RHB–MgO-2 demonstrated maximum adsorption of 79.2 mg/g at concentration of 130 mg/L, signifying its exceptional adsorption efficacy.

3.2 Nanoparticle Characterization

3.2.1 Infrared Spectra of Nanocomposites

The FT-IR data for the adsorbents (RH–MgO-1, RH–MgO-2, RHB–MgO-1, and RHB–MgO-2) are presented in Fig. 8.

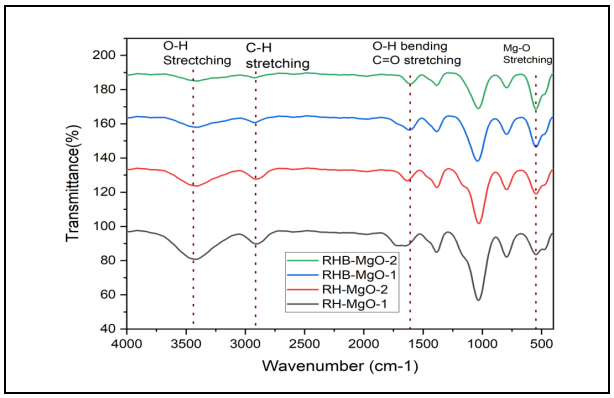

Fig. 8: FTIR spectra of prepared adsorbent composites

The FTIR spectra of the synthesized MgO–rice husk nanocomposites were recorded over the wavenumber range of 4000–400 cm^{-1} before and after Congo Red adsorption to identify the surface functional groups involved in the adsorption process. The FTIR spectra of RH–MgO-2 displayed a pronounced broad peak about 3420-3440 cm^{-1}, indicative of stretching vibration of O–H groups derived from hydroxyl functionalities in the alkali-treated rice husk. The alkali treatment increased the accessibility of hydroxyl groups by eliminating lignin, hemicellulose, and other surface contaminants (Sharmiladevi *et al.* 2024). The RH–MgO-1 sample exhibited distinct O–H and C=O stretching vibrations at roughly 3435 cm^{-1} and 1640 cm^{-1}, signifying the existence of cellulose, hemicellulose, and residual lignin functional groups. Conversely, RHB–MgO-1 and RHB–MgO-2 displayed relatively diminished O–H absorption bands attributable to the thermal degradation of hydroxyl-bearing compounds during pyrolysis, whereas the carbonaceous framework of the biochar fostered unique surface functional groups that enhanced dye adsorption. The identified oxygen- functional groups, like hydroxyl groups, were crucial in the reduction and stabilization of Mg^{2+} ions during the synthesis of MgO nanoparticles (Malkari and Boddu, 2025). Moreover, these functional groups offered several active adsorption sites for interaction with CR by hydrogen bonding, electrostatic interactions, and surface complexation, hence improving the adsorption efficacy of the synthesized MgO–rice husk nanocomposites.

3.2.2 XRD Pattern of MgO Nanoparticles

X-ray diffraction patterns of MgO nanoparticles adsorbed over RHB–MgO-2 and RH–MgO-1 are illustrated in Fig. 9 (a) and (b).

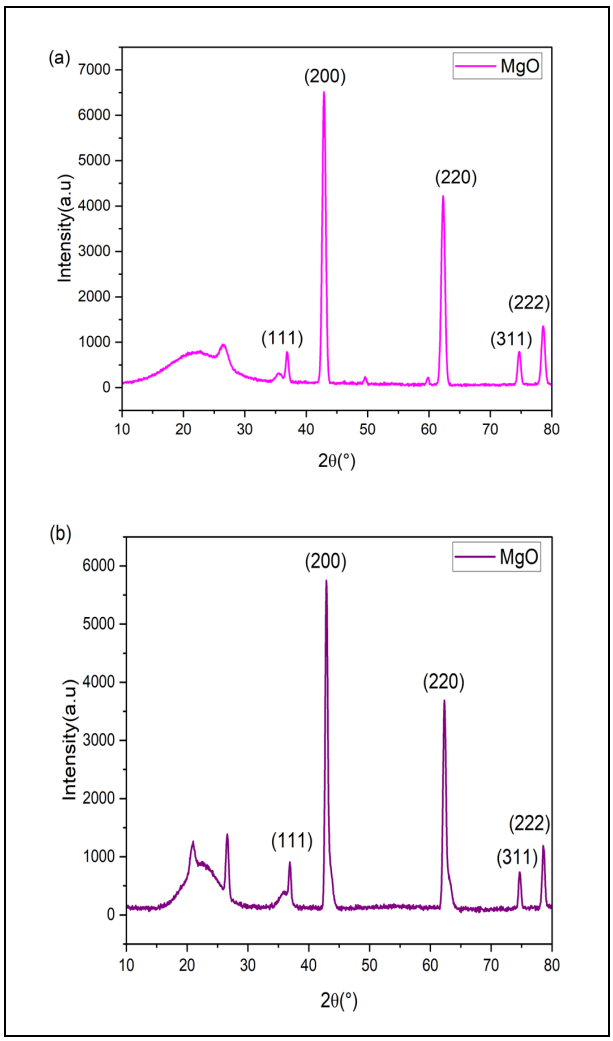

Fig. 9: (a) XRD pattern of RHB−MgO-2 and (b) XRD pattern of RH−MgO-1

The synthesized MgO–rice husk nanocomposites displayed X-ray diffraction patterns with distinct peaks at 36.9°, 42.9°, 62.3°, 74.7°, and 78.6°, which correspond to (111), (200), (220), (311), and (222) crystallographic FCC MgO, respectively. Lack of supplementary diffraction peaks signifies the great phase purity of the synthesized MgO nanoparticles, with no observable secondary crystalline phases. The distinct and well-defined peaks further validate excellent crystallinity of synthesized MgO nanocomposites. The average crystallite sizes of RH–MgO-1, RH–MgO-2, RHB–MgO-1, and RHB–MgO-2 were determined by Debye–Scherrer equation (equation 2), demonstrating effective synthesis of nanocrystalline MgO. The subtle broad diffraction features detected in the biochar-supported samples were ascribed to the amorphous carbon structure of rice husk biochar, which did not influence the crystalline characteristics of the MgO phase (Li *et al.* 2020).

$$D = \frac{K \cdot \lambda}{\beta \cdot \mathrm{Cos}\theta} \quad \ldots (2)$$

3.2.3 SEM Analysis

The SEM analysis was conducted to examine the surface morphology of the synthesized material as illustrated in Fig. 10 (a-d). The SEM micrograph revealed a rough, porous surface with numerous exposed and accessible binding sites, which are favorable for the adsorption of dye molecules.

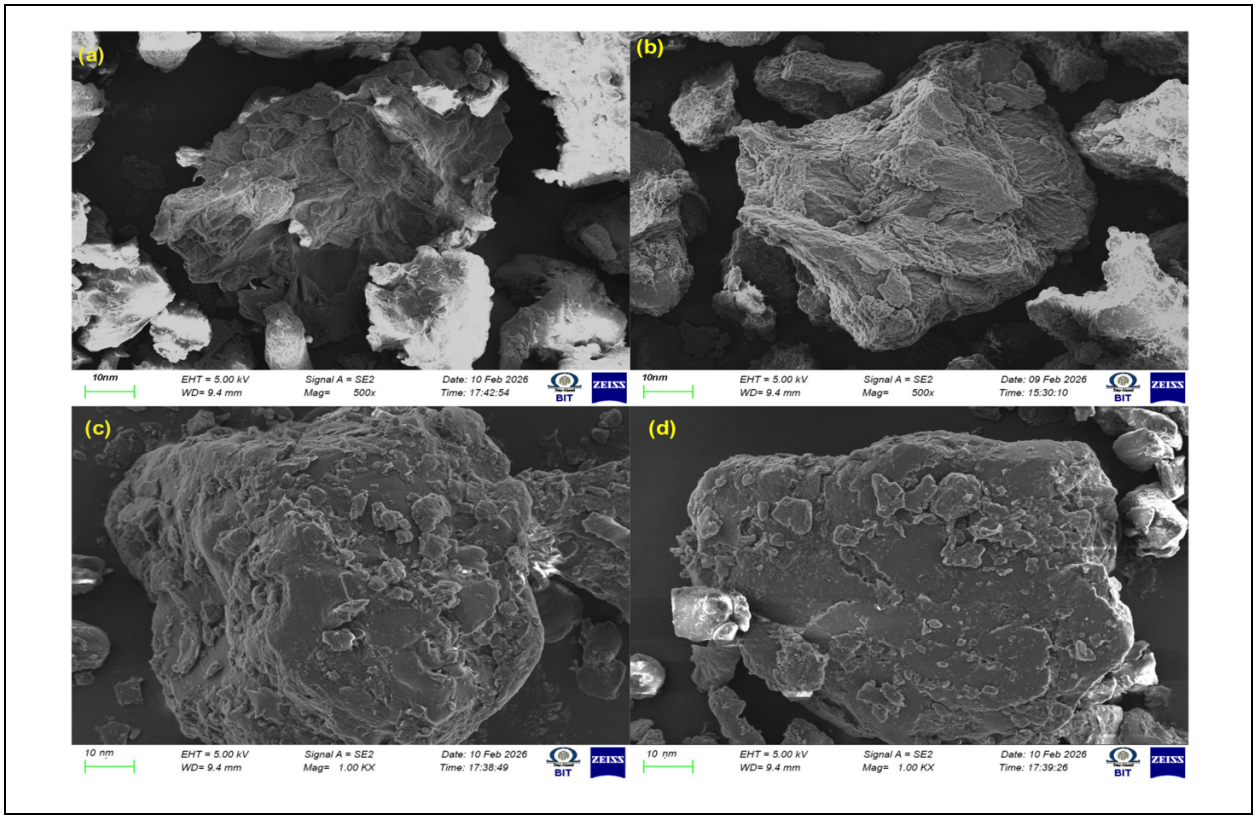

Fig. 10: SEM images of (a) RH−MgO-1 (b) RH−MgO-2 (c) RHB−MgO-1 and (d) RHB−MgO-2

3.3 Kinetic Analysis

3.3.1 Pseudo First order

The adsorption model describes the conditions governing liquid–solid adsorption and elucidates the variation in dye concentration with time, as shown in Fig. 11.

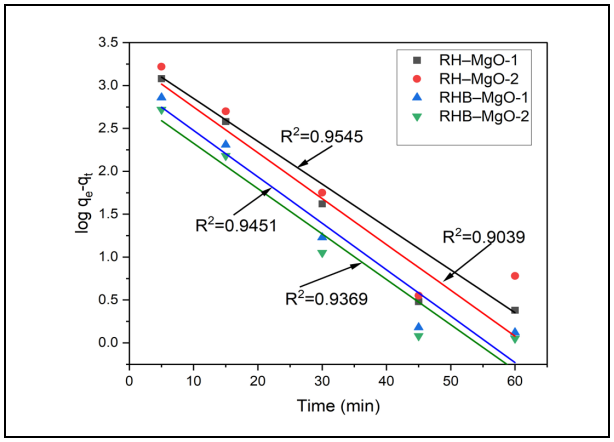

Fig. 11: Linear plot of pseudo-first-order kinetics

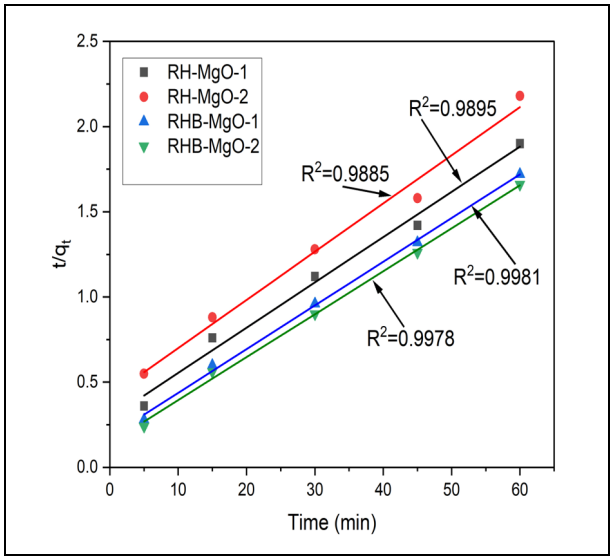

Fig. 12: Linear plot of pseudo-second-order kinetics

Equations (3 and 4) for pseudo first order are shown below (Gadore *et al.* 2023).

$$\log(q_e - q_t) = \log q_e - k_1 \frac{t}{2.303} \quad \ldots (3)$$

$$q_t = q_e(1 - e^{-K_{1.t}}) \quad \ldots (4)$$

A nonlinear equation was employed in nonlinear regression to prevent linearization. Contact duration (minutes) is t, biosorption capacity is q_e at equilibrium. Table 1 presents the correlation coefficient (R^2), k1, and the estimated and experimental biosorption for elimination of basic blue dyes.

3.3.2 Pseudo Second Order

Pseudo second-order kinetic model elucidates entire spectrum of contact time. Fig. 12 shows the linear plot of pseudo-second-order kinetics.

$$\frac{dqt}{d_t} = K_2(q_e - q_t)^2 \quad \ldots (5)$$

Pseudo second-order refers to constant for sorption (Shaikh *et al.* 2022b).

$$\left(\frac{t}{q_t}\right) = \frac{1}{K_2 qe^2} + \frac{t}{qe} \quad \ldots (6)$$

The values of R^2, K_2, qe cal and qe exp for removal of basic Congo Red are presented at Table 1.

3.3.3 Diffusion-controlled Adsorption Model

Biosorption of sorbate onto biosorbent were delineated at three principal stages of intra-particle diffusion. Initially, sorbate molecules at bulk phase adhere to surface through film diffusion. Sorbate molecules were conveyed into internal locations of biosorbent surface. Third stage entails adsorption of sorbate molecules at internal pore surfaces and central sites. Fig. 13 shows the linear Weber-Morris diffusion model plot.

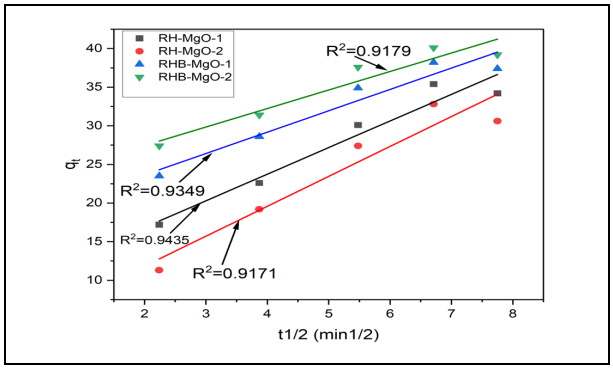

Fig. 13: Linear weber–morris diffusion model plot

The overall rate of adsorption was governed by the rate-limiting phase. Adsorption capacity was proportional to square root of contact time. The equation of the model (Kumar and Kumar, 2022) is shown below:

$$q_t = K_{pi}t^{\frac{1}{2}} + C_i \quad \ldots (7)$$

The R^2, C_i and K_{pi}, values for adsorption of basic CR dye utilizing various adsorbents is presented in Table 1.

Table 1. Kinetic model data of congo red removal

Kinetic Model	Congo Red Dye			
	RH–MgO-1	RH–MgO-2	RHB–MgO-1	RHB–MgO-2
Pseudo -1	36.8	33.9	39.4	41.8
	31.42	29.15	34.27	36.80
	0.0618	0.0564	0.0642	0.0671
	0.954	0.947	0.961	0.968
Pseudo -2	36.8	33.9	39.4	41.8
	35.91	33.46	38.52	41.05
	0.00328	0.00374	0.00312	0.00291
	0.998	0.997	0.999	0.999
Intraparticle Diffusion	3.441	3.870	2.764	2.394
	9.972	4.100	18.119	22.669
	0.9435	0.9172	0.9349	0.9180

Table 1 illustrates the relevance of different adsorption kinetic models to experimental data regarding adsorption of CR dye onto synthesized MgO–rice husk nanocomposites (RH–MgO-1, RH–MgO-2, RHB–MgO-1, and RHB–MgO-2). The computed kinetic parameters, comprising the coefficient of determination (R^2), pseudo-first (k_1), second-order rate constant (k_2), intraparticle diffusion rate constant (K_{pi}), and intercept (C_i) are presented in this table. Of the examined models, pseudo-first-order kinetic model showed the most favorable alignment to the experimental data, demonstrated by greatest R^2 and the tight correlation between experimental and estimated equilibrium adsorption. The intraparticle diffusion model demonstrated correlation coefficient ($R^2 = 0.95$). Nonetheless, failure of diffusion plots to intersect the origin shows that intraparticle diffusion was not exclusive rate-controlling factor, implying both surface adsorption and film diffusion significantly contributed to the total adsorption mechanism.

3.4 Thermodynamic Analysis

Thermodynamic analysis (Fig. 14, Table 2) elucidates the characteristics of biosorption process. Thermodynamics, including enthalpy change (ΔH_o), and

entropy change (ΔS_o) was computed utilizing biosorption thermal data for elimination of basic CR dye.

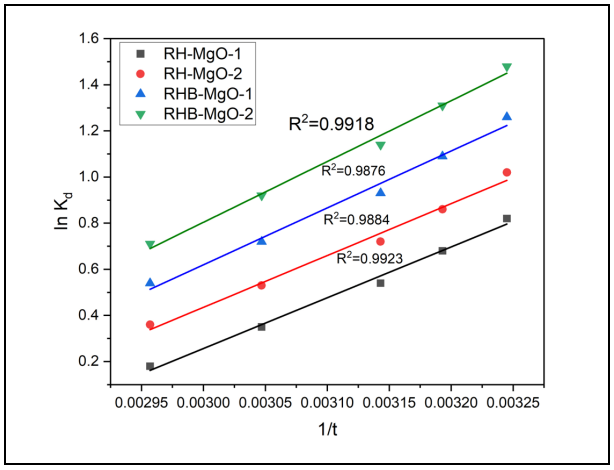

Fig. 14: Thermodynamic analysis of adsorption process

Table 2. Thermodynamic parameters of congo red

Thermodynamic Range	Temperature				
RH–MgO-1	308	313	318	328	338
RH–MgO-1 ΔG° (kJ/mol)	-2.776	-2.63	-2.378	-2.081	-1.641
ΔH° (kJ/mol)	-20.388				
ΔS° (J mol^{-1} K^{-1})	-55.996				
RH–MgO-2 ΔG° (kJ/mol)	-3.479	-3.346	-3.155	-2.881	-2.506
ΔH° (kJ/mol)	-18.544				
ΔS° (J mol^{-1}K^{-1})	-47.897				
RHB–MgO-1 ΔG° (kJ/mol)	-5.088	-4.628	-4.183	-3.679	-3.131
ΔH° (kJ/mol)	-35.504				
ΔS° (J mol^{-1} K^{-1})	-97.096				
RHB–MgO-2 ΔG° (kJ/mol)	-6.5	-5.694	-5.153	-4.563	-3.943
ΔH° (kJ/mol)	-45.584				
ΔS° (J mol^{-1} K^{-1})	-125.12				
RH–MgO-1 ΔG° (kJ/mol)	-2.776	-2.63	-2.378	-2.081	-1.641
ΔH° (kJ/mol)	-20.388				
ΔS° (J mol^{-1} K^{-1})	-55.996				

Values of ΔG_o at various temperatures was computed by subsequent equations :

$$\Delta G^o = \Delta H^o - T\Delta S^o \quad \ldots (8)$$

$$\Delta G^o = -\mathrm{RT}\ln K_d \quad \ldots (9)$$

$$\ln(K_d) = \frac{\Delta S^o}{R} - \frac{\Delta H^o}{R} \times \frac{1}{T} \quad \ldots (10)$$

The negative ΔH° values signify that adsorption of CR dye onto synthesized MgO–rice husk nanocomposites is an exothermic process, indicating that heat is liberated during the adsorption. Negative values of ΔS° signify reduction in entropy at solid–liquid throughout adsorption process, suggesting that the dye molecules attain greater order upon adsorption onto the surface of the nanocomposites. Moreover, negative ΔG° at the examined temperatures validates that the adsorption was spontaneous and thermodynamically advantageous. Value of ΔG° signifies that the adsorption of CR onto the synthesized MgO–rice husk nanocomposites happens spontaneously, without necessitating external energy input.

3.5 Adsorption Isotherm Study

Langmuir isotherm equation is presented below (Sarreshtehdar *et al.* 2023).

$$\frac{C_e}{q_e} = \frac{1}{q_m b} + \frac{C_e}{q_m} \quad \ldots (11)$$

In this context, q_m (mg/g) shows maximum biosorption capacity, whereas Langmuir constant reflects energy of biosorption. Langmuir isotherm RL were computed using the following equation (Sugumar *et al.* 2024).

$$R_L = \frac{1}{1+bC_O} \quad \ldots (12)$$

In this context, the dimensionless constant referred to as RL is the equilibrium parameter, C_o was the starting dye concentration, and b is the Langmuir constant. The RL is presented in Fig. 15. Rasilingwani *et al.* (2024) developed a nanocomposite adsorbent comprising MgO nanoparticles embedded in bentonite clay for the treatment of dye-contaminated wastewater. The adsorbent achieved ≥99% CR removal at a dosage of ≤1 g L^{-1} within 10 minutes. The adsorption data fitted the Langmuir isotherm ($R^2 \geq 0.99$) and followed a pseudo-second-order kinetic model. Furthermore, approximately 100% CR removal was achieved from real printing-ink wastewater.

Table 3. Interpretation of the langmuir separation factor (R_l) for adsorption favorability

R_L Values	$R_{L=0}$	$0 < R_L < 1$	$R_{L>1}$
Nature		irreversible	Unfavorable

Table 4. Removal of basic congo red dye

Model	RH–MgO-1	RH–MgO-2	RHB–MgO-1	RHB–MgO-2
Langmuir	44.7	58.2	73.8	79.2
	55.84	68.97	81.97	92.59
	0.243	0.116	0.167	0.111
	0.039	0.095	0.062	0.100
	0.9410	0.9906	0.9395	0.9115
Freundlich	17.81	18.96	20.37	21.12
	2.01	2.85	2.74	3.18
	2.12	2.68	2.31	2.54
	0.9445	0.9776	0.9636	0.9821
Temkin	48.20	63.80	73.80	78.50
	1.86	2.42	2.95	3.38
	16.54	19.62	21.84	22.67
	0.9785	0.9792	0.9865	0.9650
Dubinin-Radushkevich	17.10	18.54	20.14	21.35
	8.34	6.97	5.88	5.12
	7.74	8.47	9.22	9.88
	0.9369	0.9511	0.9224	0.9256
Harkins- Jura	55.84	68.47	81.97	92.59
	0.52	0.44	0.36	0.29
	2.11	1.92	1.64	1.28
	0.9481	0.8642	0.9630	0.9685

3.5.1 Linear Freundlich Model

This model posits that biosorption occurs across multiple layers, indicating that adsorption on the biosorbent surface is heterogeneous and that the sorbed molecules interact with sites of varying affinities.

$$\log q_e = \log K_F + \frac{1}{n}\log C_e \qquad \dots (13)$$

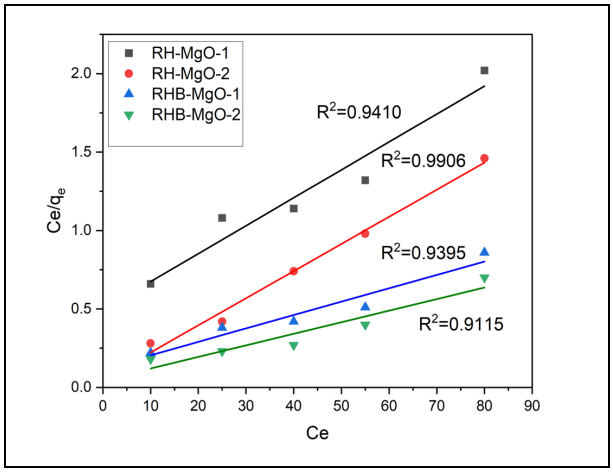

Fig. 15: Adsorption langmuir analysis

Freundlich constants were empirical and values fluctuated based on many environmental circumstances. Unit value of n signifies linear biosorption; a number below one implies a chemical process nature of biosorption, while value above one denotes a biosorption process. K_F and n were derived by graphing linear graph (Table 3 and Fig. 16).

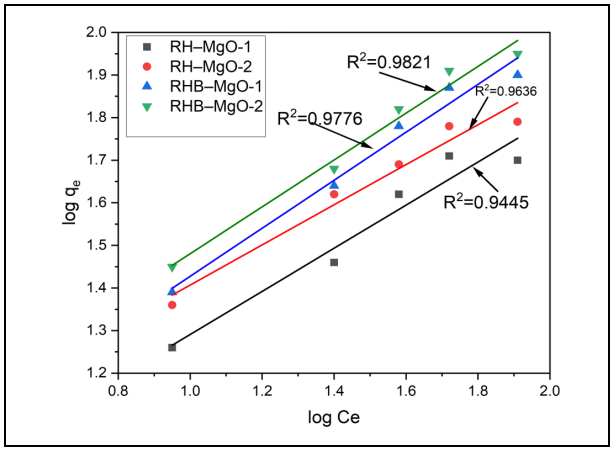

Fig. 16: Linear freundlich model

The Temkin isotherm is based on two main assumptions. First, the heat of adsorption decreases linearly with increasing surface coverage due to interactions between the adsorbate and the biosorbent surface. Second, the binding energies of the adsorbate molecules are assumed to be uniformly distributed across the available adsorption sites on the biosorbent surface.

$$qe = \text{Bln}\, A + \text{Bln}\, C_e \qquad \dots (14)$$

The Temkin constant was marked by A, and B signifies constant. R (8.222 J mol^{-1} K^{-1}) was gas constant. Graphical representation of Temkin isotherm is illustrated in Fig. 17.

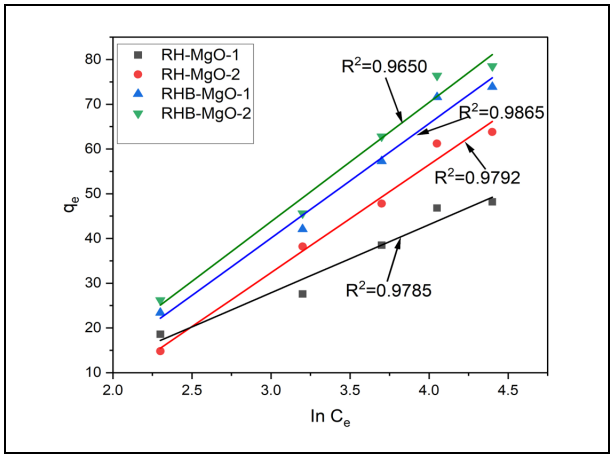

Fig. 17: Linear temkin model

$$\frac{1}{qe^2} = \left(\frac{B}{A}\right) - \left(\frac{1}{A}\right)\log C_e \quad \ldots (15)$$

The Harkin Jura isotherm is represented by A, whereas B is constant in the specified equation, as detailed in Table 4 and Fig. 18.

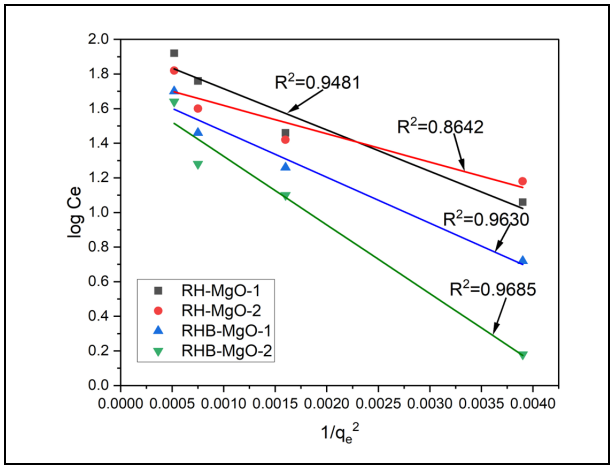

Fig. 18: Linear harkins–jura model

3.5.2 Dubinin-Radushkevich Model

The enhanced desorption observed with hydrochloric acid can be attributed to the higher concentration of H^+ ions, which compete with the adsorbed CR molecules for active adsorption sites on the MgO–rice husk nanocomposites. Isotherm was used to evaluate the nature of biosorption and the mean adsorption energy. This model describes the relationship between the equilibrium concentration of the adsorbate and the amount of adsorbate biosorbed at equilibrium.

$$\ln q_e = \ln q_m - \beta\varepsilon^2 \quad \ldots (16)$$

The theoretical saturation is denoted as q_m, and the Polanyi potential is represented by ε. The constant associated with biosorption energy is β.

$$\varepsilon = R\mathrm{T}\ln\left(1 + \frac{1}{C_e}\right) \quad \ldots (17)$$

Here, absolute temperature is denoted as T (K) and gas constant as R (8.314 J mol^{-1} K^{-1}.

$$E = 1/_{(2\beta)}1/2 \quad \ldots (18)$$

The correlation coefficient (R^2) is presented in Table 4 and Fig. 19.

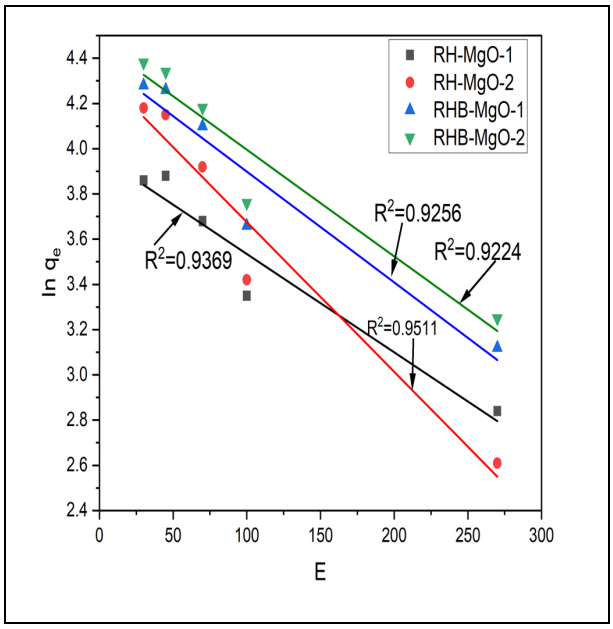

Fig. 19: D–R adsorption model analysis

The adsorption equilibrium was examined by many adsorption isotherms to assess their suitability for characterizing adsorption of Congo Red dye onto MgO–rice husk nanocomposites (RH–MgO-1, RH–MgO-2, RHB–MgO-1, and RHB–MgO-2). The appropriateness of each isotherm model was evaluated by comparing experimentally obtained highest adsorption capacity with calculated adsorption capacity with the respective coefficient of determination (R^2).

Table 4 demonstrates that the Langmuir isotherm model yielded optimal match for adsorption equilibrium data of all four MgO–rice husk nanocomposites. The strong correlation between observed and estimated adsorption capabilities, along with the elevated R^2 values, suggests that the adsorption of CR primarily took place *via* monolayer adsorption on uniform surface with energetically similar active sites. Conversely, Freundlich isotherm model demonstrated relatively lower correlation coefficients, indicating its diminished appropriateness for characterizing the adsorption behavior. The Temkin isotherm model

exhibited a satisfactory match, signifying impact of adsorbent–adsorbate throughout adsorption process. The Dubinin–Radushkevich and Harkins–Jura isotherm models exhibited inadequate concordance with experimental results, indicating their unsuitability for characterizing desorption equilibrium of CR dye onto the synthesized MgO–rice husk nanocomposites.

3.6 Electrolyte Effect on Dye Biosorption

The substantial amounts of inorganic salts are typically employed to improve dye fixing, leading to effluent with elevated levels of dissolved electrolytes. Consequently, examining the impact of electrolytes on the adsorption efficacy of adsorbents is crucial for determining their practical utility in wastewater treatment. This study examined three prevalent electrolytes, specifically $AlCl_3{\cdot}6H_2O$, NaCl and $CaCl_2{\cdot}2H_2O$, at concentrations of 0.05 - 0.50 M to assess the affect on adsorption efficacy of the synthesized MgO–rice husk nanocomposites regarding CR dye (Fig. 20).

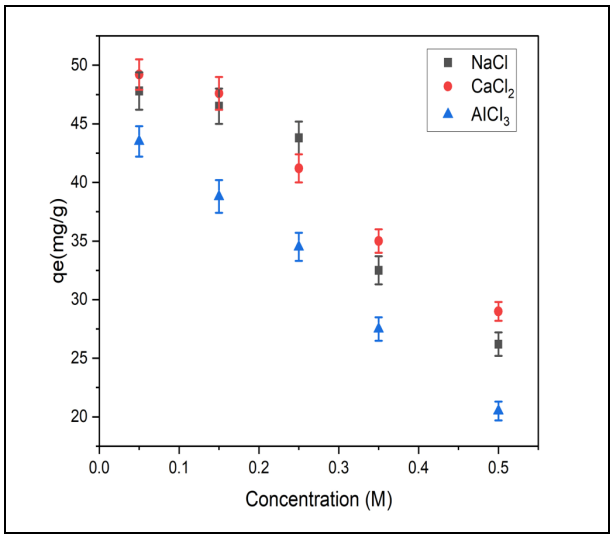

Fig. 20: Effect of electrolytes on adsorption

Electrolytes in ionic state generate occasionally repulsive attractive interactions among salt ions and dye molecules. Consequently, adsorption of dye onto adsorbent surface diminishes. Significantly as salt content rises, the adsorption capability diminishes.

3.7 Effect on Heavy Metal Ions

Heavy metal ions at textile effluent can markedly affect the adsorption efficacy of adsorbents by competing with dye molecules for accessible active sites. To assess this effect, varying concentrations (40–200 ppm) of chromium and lead ions were added to Congo Red dye solution, and their impact on the adsorption efficiency of the synthesized MgO–rice husk nanocomposites was examined (Fig. 21). Findings indicated heavy metal ions negatively impacted adsorption of CR dye. With raise in concentration of Cr and Pb ions, adsorption capabilities of all four nanocomposites progressively diminished. This decrease is due to the competitive adsorption of heavy metal ions and dye for identical adsorbent surface, hence restricting availability of sites for dye adsorption. As a result, all four MgO–rice husk nanocomposites showed a marked reduction in adsorption capacity when exposed to heavy metal ions, indicating that inclusion of metal ions significantly affects adsorption efficacy of the synthesized adsorbents.

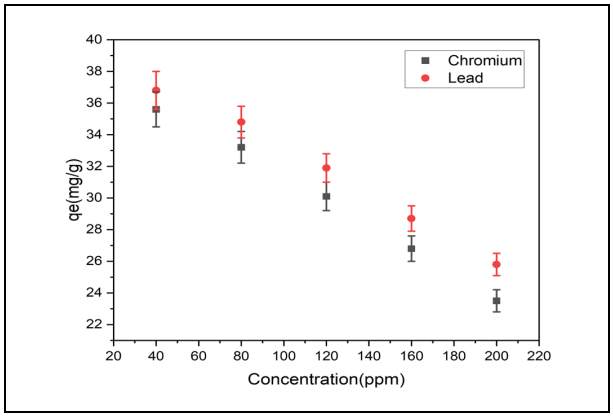

Fig. 21: Effect of heavy metal ions

3.8 Reusability and Desorption Assessment

Reusability of adsorbent is a critical attribute, as it influences its capacity for repeated application and its economic viability in extensive wastewater treatment processes. The regeneration and reutilization of adsorbents save operational expenses and mitigate the production of secondary waste. Consequently, choosing a suitable desorbing agent (eluent) is crucial for effective renewal of the adsorbent. This work assessed the efficacy of acetic acid solutions and 0.50 N HCl in desorbing CR dye from the synthesized MgO–rice husk nanocomposites. The desorption results are illustrated in Fig. 22(a) and 22(b).

The findings indicated that 0.50 N HCl served as the most efficacious eluent, yielding maximum desorption efficiencies of 95.7% for RH–MgO-1, 97.3% for RH–MgO-2, 91.2% for RHB–MgO-1, and 92.4% for RHB–MgO-2. Moreover, increasing the eluent concentration from 0.05 N to 0.50 N gradually enhanced the desorption efficiency of all four nanocomposites.

The enhanced desorption observed with hydrochloric acid can be attributed to the higher concentration of H^+ ions, which compete with the adsorbed CR molecules for active adsorption sites on the MgO–rice husk nanocomposites. This competitive ion-exchange mechanism diminishes the contact between the adsorbent and dye, hence promoting the desorption of

dye molecules at adsorbent surface. Elevated desorption efficiency achieved post-regeneration suggests that the synthesized MgO–rice husk nanocomposites exhibit remarkable reusability and are viable options for recurrent wastewater treatment applications.

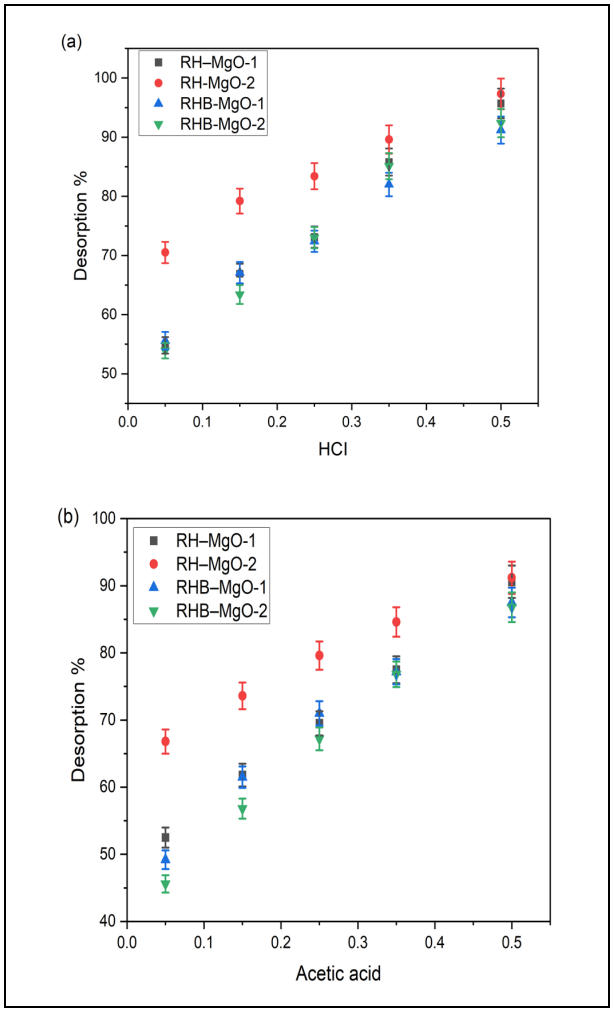

Fig. 22: (a) HCl-induced desorption efficiency and (b) Acetic acid-induced desorption efficiency

4. CONCLUSION

This study successfully synthesized MgO nanoparticles *via* a green method utilizing rice husk-derived materials. The adsorption efficacy for Congo Red dye was systematically examined. The effective synthesis of MgO–rice husk nanocomposites was validated using FTIR, XRD, and SEM investigations. Under optimum operating conditions of 0.05 g adsorbent dose, 1 hour contact time, and 35 °C, adsorption capacities of RH–MgO-1, RH–MgO-2, RHB–MgO-1, and RHB–MgO-2 were 44.7, 58.2, 73.8, and 79.2 mg/g, respectively. The ideal pH levels for optimal adsorption was 8 for RH–MgO-1, 9 for RH–MgO-2, and 10 for both RHB–MgO-1 and RHB–MgO-2.

Adsorption kinetics were optimally characterized by pseudo-first-order model, exhibiting R^2 between 0.80 and 0.95, while the strong correlation between experimental and estimated equilibrium adsorption capacities validated the appropriateness of the kinetic model. Thermodynamic research with adsorption process was exothermic and spontaneous, as demonstrated by negative ΔG° values across the temperature range 308–338 K and negative ΔH° values between −20.388 and −55.996 kJ/mol.

The synthesized nanocomposites showed superior adsorption efficiency, commendable regeneration potential, and advantageous thermodynamic properties. The use of plentiful agricultural waste (rice husk) in conjunction with MgO nanoparticles offers eco-friendly, cost-effective, and adsorbent system with potential for the effective removal of Congo Red from textile effluents.

FUNDING

This research received no specific grant from any funding agency in the public, commercial, or not-for-profit sectors.

CONFLICTS OF INTEREST

The authors declare that there is no conflict of interest.

COPYRIGHT

This article is an open-access article distributed under the terms and conditions of the Creative Commons Attribution (CC BY) license (http://creativecommons.org/licenses/by/4.0/).

REFERENCES

Abdallah, M. A. M. and Alprol, A. E., Utilization of aquatic biomass as biosorbent for sustainable production of high surface area, nano- microporous, for removing two dyes from wastewater, *Sci. Rep.*, 14(1), 4471 (2024). https://doi.org/10.1038/s41598-024-54539-2

Abou, O. H., Abdellaoui, Y., Laabd, M., El Ouardi, M., Brahmi, Y., Iazza, M. and Abou, O. J., Eco-efficient green seaweed codium decorticatum biosorbent for textile dyes: Characterization, mechanism, recyclability, and rsm optimization, *ACS Omega*, 5(35), 22192–22207 (2020). https://doi.org/10.1021/acsomega.0c02311

Albouyeh, A., Pourahmad, A. and Kefaya, H., Green synthesis of magnesium oxide nanoparticles in MFI type zeolite and its application as a photocatalyst, *J. Water Environ. Nanotechnol.*, 5(3), 283–293 (2020). https://doi.org/10.22090/jwent.2020.03.008

Alfajri, B., Daffalla, S., Alzouraiq, H., Bin Maan, S., Alfuzaya, A. and El-Aassar, M. R., MgO Nanoparticles-Functionalized Palm Leaf Biochar for Efficient and Sustainable Congo Red Removal, *J. Compos. Sci.*, 10(5), 270 (2026). https://doi.org/10.3390/jcs10050270

Alghanmi, R. M. and Abdelrahman, E. A., Simple production and characterization of ZnO/MgO nanocomposite as a highly effective adsorbent for eliminating congo red dye from water-based solutions, *Inorg. Chem. Commun.*, 161, 112137 (2024). https://doi.org/10.1016/j.inoche.2024.112137

Ali, M. and Dreaa, A. A. A., Green synthesis of nano binary oxide MgO/SiO_2 antibiotic, cytotoxicity and applied on wound dressing, *Egypt. J. Chem.*, 66(5), 369–377 (2023). https://doi.org/10.21608/EJCHEM.2022.148301.6413

Ameen, S. S. M., Algethami, F. K., Ahmed, S. S., Ahmed, I. I., Abdelhamid, H. N. and Omer, K. M., Bio-inspired manganese nanoparticles from pine needles with enhanced adsorptive performance, *New J. Chem.*, 50(4), 1880–1891 (2026). https://doi.org/10.1039/d5nj04047g

Begum, A. H., Savitha, S., Vidaarth, T. M. N., Jagan, K. S. G., Surendhiran, S., Karthik, A. and Kalpana, B., Design and optimization of Ag decorated MgO nanosphere catalyst for efficient removal of textile industry pollutants and their biological applications, *J. Ind. Chem. Soc.*, 102(2), 101573 (2025). https://doi.org/10.1016/j.jics.2025.101573

Gaddala, B., Devi, K. V., Balakrishnan, V., Sundramurthy, V. P., Hariprabhu, M., Mayakannan, S., Kadaikunnan, S. and Khaled, J. M., Evaluation of detoxification performance of Pithecellobium dulce seed pod powder upon acid treatment: removal of reactive red 195-A dye and kinetic analysis, *Zeitschrift für Physikalische Chemie*, 239(6), 885–910 (2025). https://doi.org/10.1515/zpch-2024-0879

Gadore, V., Mishra, S. R. and Ahmaruzzaman, M., Bio-inspired sustainable synthesis of novel SnS_2/biochar nanocomposite for adsorption coupled photodegradation of amoxicillin and congo red: Effects of reaction parameters, and water matrices, *J. Environ. Manage.*, 334, 117496 (2023). https://doi.org/10.1016/j.jenvman.2023.117496

Güllüce, E., Gülşahin, Y., Karadayı, G., Karadayı, M. and Güllüce, M., Bio-removal and Detoxification of Congo Red Dye in Aqueous Solutions by Using a Sustainable Biosorbent from Robinia pseudoacacia L., *Int. J. Environ. Res.*, 20(3), 135 (2026). https://doi.org/10.1007/s41742-026-01086-5

Guo, T. and Bulin, C., Facile preparation of MgO/graphene oxide nanocomposite for efficient removal of aqueous Congo red: adsorption performance and interaction mechanism, *Res. Chem. Intermed.*, 47(3), 945–971 (2021). https://doi.org/10.1007/s11164-020-04310-9

Gupta, A. and Dey, P., Hydrothermal and NaOH-treated rice straw fibre: A potential lignocellulosic biosorbent material for removal of textile dyes from contaminated industrial wastewater, *Int. J. Biol. Macromol.*, 305, 141109 (2025). https://doi.org/10.1016/j.ijbiomac.2025.141109

Inam, H., Durrani, A. I., Huma, R. and Hussain, F., Leaves extracts-driven synthesis of ZnO nanoparticles for enhanced adsorption of methyl red dye, *Chem. Pap.*, 79(9), 5921–5940 (2025). https://doi.org/10.1007/s11696-025-04163-9

Khader, E. H., Mohammed, T. J. and Albayati, T. M., Comparative performance between rice husk and granular activated carbon for the removal of azo tartrazine dye from aqueous solution, *Desalin. Water Treat.*, 229, 372–383 (2021). https://doi.org/10.5004/dwt.2021.27374

Khasim, S., Dastager, S. G., Alahmdi, M. I., Hamdalla, T. A., Ulla, M. F., Panneerselvam, C. and Makandar, M. B., Green synthesis of multifunctional Cu/MnO@Biochar 3D structure as a high-performance anode material in Li-ion batteries and oxidative removal of Congo red dye, *Case Stud. Chem. Environ. Eng.*, 9, 100561 (2024). https://doi.org/10.1016/j.cscee.2023.100561

Kumar, P. A. and Kumar, M. M., Green synthesis of Fe_3O_4-onion peel biochar nanocomposites for adsorption of Cr(VI), methylene blue and congo red dye from aqueous solutions, *J. Mol. Liq.*, 349, 118161 (2022). https://doi.org/10.1016/j.molliq.2021.118161

Li, P., Lin, Y., Chen, R. and Li, W., Construction of a hierarchical-structured MgO-carbon nanocomposite from a metal-organic complex for efficient CO_2 capture and organic pollutant removal, *Dalton Trans.*, 49(16), 5183–5191 (2020). https://doi.org/10.1039/d0dt00722f

Malkari, K. R. and Boddu, S., Advanced photocatalysis with biochar-TiO_2 composite for efficient oxidation of Congo red dye, *Environ. Monit. Assess.*, 197(7), 831 (2025). https://doi.org/10.1007/s10661-025-14290-1

Mayakannan, S., Rathinam, R., Saminathan, R., Deepalakshmi, R., Gopal, M., Hillary, J. J. M., Nanthakumar, S., Ganvir, V. Y. and Singh, P., Analysis of Spectroscopic, Morphological Characterization and Interaction of Dye Molecules for the Surface Modification of TiB_2 Nanoparticles, *J. Nanomater.*, 2022(1), 1033216 (2022). https://doi.org/10.1155/2022/1033216

Modwi, A., Khezami, L., Ghoniem, M. G., Nguyen-Tri, P., Baaloudj, O., Guesmi, A., AlGethami, F. K., Amer, M. S. and Assadi, A. A., Superior removal of dyes by mesoporous MgO/g-C_3N_4 fabricated through ultrasound method: Adsorption mechanism and process modeling, *Environ. Res.*, 205, 112543 (2022). https://doi.org/10.1016/j.envres.2021.112543

Nguyen, D. T. C., Dang, H. H., Vo, D.-V. N., Bach, L. G., Nguyen, T. D. and Tran, T. V., Biogenic synthesis of MgO nanoparticles from different extracts (flower, bark, leaf) of Tecoma stans (L.) and their utilization in selected organic dyes treatment, *J. Hazard. Mater.*, 404, 124146 (2021). https://doi.org/10.1016/j.jhazmat.2020.124146

Rajesh, Y., Gautam, N., Shah, J., Thandlam, A. K., Gole, S., Nirgude, P. and Dabhade, G., Evaluation of Activated Biochar from Sustainable *Sterculia foetida* Shells for the Removal of AB 158 Dye, *J. Environ. Nanotechnol.*, 13(2), 248-255 (2024). https://doi.org/10.13074/jent.2024.06.242607

Raman, G., Kumar, U. S., Vasumathi, V. and Muthu, K., Improving photocatalytic performance of nickel oxide infused chitosan nanocomposite for adsorption of organic dyes, *Surf. Interf.*, 56, 105505 (2025). https://doi.org/10.1016/j.surfin.2024.105505

Rasilingwani, T. E., Gumbo, J. R., Masindi, V. and Foteinis, S., Removal of Congo red dye from industrial effluents using metal oxide-clay nanocomposites: Insight into adsorption and precipitation mechanisms, *Water Res. Ind.*, 31, 100253 (2024). https://doi.org/10.1016/j.wri.2024.100253

Ravikumar, M. and King, P., Application of response surface optimization on biosorption of congo red dye onto spathodea campanulata leaves, *Desalin. Water Treat.*, 182, 342–350 (2020). https://doi.org/10.5004/dwt.2020.25140

Sabherwal, H., Kumar, R., Yadav, S., Sirohi, H. and Kataria, N., Green synthesis of graphene-like porous carbon (GPC) for the adsorption of pharmaceutical traces from an aquatic system: predicting the performance by machine learning and response surface methodology, *Int. J. Environ. Anal. Chem.*, 106(10), 3215-3240 (2026). https://doi.org/10.1080/03067319.2025.2608250

Sarreshtehdar, A. H., Poursattar, M. A. and Gozali, B. P., Pelargonium as a cost-effective Additive in Bio-composite Adsorbent in Removing dyes from Wastewater: Equilibrium, Kinetic, and Thermodynamic studies, *J. Polym. Environ.*, 31(7), 3230–3247 (2023). https://doi.org/10.1007/s10924-023-02794-1

Sasikumar, P., Mohanaparameswari, S., Balachandramohan, M., Silambarasan, T., Arularasu, M. V. and Vimalan, M., Green Synthesis and Characterization of Ag_2O/MgO/Rice Husk Ash Hybrid Composite: Structural, Dielectric and Antibacterial Applications, *Waste Biomass Valoriz.*, 17(7), 3821–3834 (2026). https://doi.org/10.1007/s12649-025-03328-7

Şentürk, İ. and Topal, C. G., Green synthesis of CuO adsorbent using Polygonum sivasicum for efficient adsorptive removal of tetracycline hydrochloride, *Int. J. Environ. Sci. Technol.*, 23(1), 30 (2026). https://doi.org/10.1007/s13762-025-06910-7

Shaikh, W. A., Chakraborty, S., Islam, R. U., Ghfar, A. A., Naushad, M., Bundschuh, J., Maity, J. P. and Mondal, N. K., Fabrication of biochar-based hybrid Ag nanocomposite from algal biomass waste for toxic dye-laden wastewater treatment, *Chemosphere*, 289, 133243 (2022a). https://doi.org/10.1016/j.chemosphere.2021.133243

Shaikh, W. A., Kumar, A., Chakraborty, S., Islam, R. U., Bhattacharya, T. and Biswas, J. K., Biochar-based nanocomposite from waste tea leaf for toxic dye removal: From facile fabrication to functional fitness, *Chemosphere*, 291, 132788 (2022b). https://doi.org/10.1016/j.chemosphere.2021.132788

Sharmiladevi, S., Ramesh, N., Prabhu, S. V. and Mayakannan, S., Microwave-assisted functionalized biosorbent preparation using seed gum of Tamarindus indica: characterization and evaluation of Cr(VI) removal potency from tannery effluents, *Biomass Convers. Biorefine.*, 14(12), 13533–13545 (2024). https://doi.org/10.1007/s13399-024-05667-2

Sugumar, M., Bharathi, S., Sampath, V., Sundramurthy, V. P., Selvaraju, M., Kadaikunnan, S. and Khaled, J. M., Biosorption of Pb(II) ions through nanostructured teff straw based magnetized activated biocarbon: Aspects on modeling, optimization, and kinetics, *Global Nest J.*, 26(9), 06479 (2024). https://doi.org/10.30955/GNJ.06479